Optimal Reconfiguration of Power Distribution Grids to Maintain Line Thermal Efficiency During Progressive Wildfires

Mehdi Rostamzadeh, *Student Member, IEEE*, Mohammad Heidari Kapourchali, *Member, IEEE*, Long Zhao, *Member, IEEE*, and Visvakumar Aravinthan, *Senior Member, IEEE*

***Abstract*—The worsening wildfires due to intensified climate variability increases the risk of both unplanned power outages as well as planned power line de-energizations. It is because wildfires cause thermal stress on overhead conductors, which harms the mechanical properties of overhead distribution lines. This article proposes a proactive strategy for improving the operational efficiency and decision-making capabilities of power distribution networks under progressive wildfire conditions. Dynamic heat balance equations are used to characterize the effect of wildfire on the overhead line conductors. The optimal dynamic reconfiguration of the distribution system and the operation of backup generators are considered as tools to minimize the curtailed loads while maintaining the maximum flow of current through the lines within the thermal rating of the line conductors. A mixed-integer conic programming model is adopted to minimize the operation and load curtailment costs. A higher value of lost load is applied to enhance the continuity of the electricity supply to critical loads. The proposed framework is tested under various environmental conditions and wildfire paths using both a modified 33-node network and the practical 83-node Taiwan Power Company's distribution grid. Results show that the proposed approach enhances proactive decision-making for power distribution system operations and increases the resilience of critical loads to wildfire threats.**

***Index Terms*—Heat gain, heat loss, mixed-integer conic programming, power distribution grid reconfiguration, thermal rating, wildfire.**

NOMENCLATURE

Indices and Sets

ij	Line index connecting node i to node j.
i,j	Node indices.
$\Psi_L/\Psi_B/\Psi_{EG}$	Set of lines/nodes/nodes with emergency generators (EGs).
$\mathcal{N}(i)$	Set of nodes connected to node i by a line.

Parameters and Constants

L	Flame length $[\mathrm{m}]$.
W	Flame width $[\mathrm{m}]$.
γ	Flame tilt angle [degree].
T_f	Flame zone temperature $[^\circ\mathrm{K}]$.
ε_{FZ}	Flame zone emissivity.
ρ_b	Fuel bulk density $[\mathrm{kg/m^3}]$.
r_{fr}^0	Initial distance of fire from the line $[\mathrm{m}]$.
T_a	Ambient temperature $[^\circ\mathrm{C}]$.
V_{wind}	Wind speed $[\mathrm{m/s}]$.
θ_{wind}	Angle between the wind direction and the conductor axis [degree].
θ_s	Effective angle of the Sun's rays [degree].
Q_s	Solar and sky radiated heat flux intensity $[\mathrm{W/m^2}]$.
τ	Dimensionless atmospheric transmissivity.
ρ_a	Density of air $[\mathrm{kg/m^3}]$.
μ_a	Dynamic air viscosity [kg/ms].
∂_B	Stefan-Boltzmann constant $[\mathrm{W/m^2K^4}]$.
A'	Projected area of conductor per unit length $[\mathrm{m^2/m}]$.
D_c	Conductor diameter $[m]$.
ε_c	Conductor emissivity.
h_L	Vertical position of the line $[m]$.
g_{ij}	Conductance of line between node i and j.
b_{ij}	Susceptance of line between node i and j.
b_{ij}^{sh}	Shunt susceptance of line between node i and j.
$T_c^{\max}$	Maximum allowable conductor temperature $[^\circ\mathrm{C}]$.
α_{Sun}	Solar absorptivity.
k_a	Air thermal conductivity.
N_{Re}	Reynolds number.
P_i^D	Active power demand at node i.
Q_i^D	Reactive power demand at node i.
$\mathcal{C}^{\text{EG}}$	EGs generation price ($/MWh).
$\mathcal{C}^{\text{grid}}$	Power price of the upstream network ($/MWh).

Manuscript received 31 May 2023; revised 16 September 2023; accepted 23 November 2023. Date of publication 19 December 2023; date of current version 15 March 2024. The work of UAA was supported in part by the U.S. National Science Foundation under Grants RISE-2220624 and RISE-2022705. *(Corresponding author: Mehdi Rostamzadeh.)*

Mehdi Rostamzadeh is with the Department of Electrical and Computer Engineering, Wichita State University, Wichita, KS 67260 USA (e-mail: mxrostamzadeh@shockers.wichita.edu).

Mohammad Heidari Kapourchali is with the Department of Electrical Engineering, University of Alaska Anchorage, Anchorage, AK 99508 USA, and also with the Alaska Center for Energy and Power, Fairbanks, AK 99775 USA (e-mail: mhkapourchali@alaska.edu).

Long Zhao is with the Department of Electrical Engineering and Computer Science, South Dakota School of Mines and Technology, Rapid City, SD 57701 USA (e-mail: long.zhao@sdsmt.edu).

Visvakumar Aravinthan is with the Department of Electrical and Computer Engineering, Wichita State University, Wichita, KS 67260 USA (e-mail: visvakumar.aravinthan@wichita.edu).

Digital Object Identifier 10.1109/JSYST.2023.3339771

VoLL	Value of lost load ($/MWh).
R	Conductor resistance (Ω/m).

Variables and Dependent Quantities

V_{fr}	Fire rate of spread $[\mathrm{m/s}]$.
r_{fr}	Fire distance from the line $[\mathrm{m}]$.
ϑ_{fr}	The angle ahead the flame.
φ_{frr}	Fire radiative heat flux $[\mathrm{W/m^2}]$.
T_c	Conductor temperature $[^\circ\mathrm{C}]$.
$\mathcal{H}_\mathrm{s}$	Heat transfer rate from sun to conductor $[\mathrm{W/m}]$.
$\mathcal{H}_{cf}/\mathcal{H}_{rf}$	Convective/Radiative heat transfer rate from fire to conductor $[\mathrm{W/m}]$.
$\mathcal{H}_c/\mathcal{H}_r$	Convective/Radiative heat loss rate of conductor $[\mathrm{W/m}]$.
P_i^{inj}	Active power injection at node i.
Q_i^{inj}	Reactive power injection at node j.
P_{ij}	Active power flow from node i to node j.
Q_{ij}	Reactive power flow from node i to node j.
I_{ij}	Current magnitude through line ij.
$\mathcal{Y}_{ij}$	Status of line between node i and j.
$V_i,\ V_j$	Voltage magnitude of node i and j.
$\mathcal{V}_i$	Conic voltage variable at node i.
$\mathcal{V}_i^{ij}$	Conic voltage variable for node i and line ij.
$\mathcal{R}_{ij}/\mathcal{T}_{ij}$	Conic variables for line ij.
P_i^{EG}	EGs active power generation at node i .
Q_i^{EG}	EGs reactive power generation at node i .
P^{grid}	Power exchange with the upstream network.

Symbols

$(\bar{\bullet})/(\underline{\bullet})$	Upper/lower limit of variable/parameters.

I. Introduction

WILDFIRES have increased in frequency and intensity in recent years, posing new and emerging risks to infrastructures and communities. In 2018, British Columbia experienced its worst fire season on record with 2115 fires and 1.35 million hectares burned surpassing 2017's fire season, previously the largest recorded burned area [1]. An unprecedented fire season ravaged Australia in 2019–2020, destroying 3113 houses and burning 19 million hectares [2]. Between 2017 and 2020, more than 200 000 wildfires have burned over 25 million acres in the U.S. [3]. The Annual Wildfires Report from the National Centers for Environmental Information indicates that over 7 million acres of wildland were burned by fire only in 2021 [4]. According to the National Climate Assessment, the size of the area burned in Alaska's wildfires is projected to double by 2050 and triple by 2100 under continued emissions and further warming [5]. The U.S. Forest Service's spending on wildfires has increased from 16 percent in 1995 to more than 50 percent of the agency's annual budget in 2015 [6]. The U.S. Department of Commerce estimates the total annualized cost of wildfires to be between $71.1 billion and $347.8 billion, including direct structural losses and rebuilding, as well as indirect costs [7].

As wildfires become more widespread and prolonged, the availability of critical infrastructures such as power [8], water [9], and communication [10] networks become more vital for societal response to such threatening events. Wildfires have substantial impacts on power grids, and strategies to enhance the resilience of power systems have recently drawn significant attention. Substantial effort has been made to prevent wildfires. Muhs et al. [11] demonstrate increased fault probability due to line congestion and overloading and propose an analytical framework that can be used to evaluate long-term and short-term solutions for reducing wildfire ignitions in power distribution systems. Tandon et al. [12] demonstrates the practical application of dynamic line ratings and the enforcement of more stringent ground clearance criteria for transmission lines. These measures are employed to regulate current flows on lines that pose a heightened risk of wildfire ignition. Through the management of current flow within the lines, Muhs et al. [11] and Tandon et al. [12] seek to reduce the probability of power grid-induced wildfires. Nevertheless, they do not account for scenarios where the power grid faces the threat of an approaching wildfire.

A range of grid hardening strategies, such as overhead structure reinforcement, vegetation management, prescribed burning, and undergrounding, are also used to bolster the resilience of the power grid [13], [14]. However, they are considered as long-term solutions to enhance the resilience of the electric utilities against wildfires. To offer real-time solutions, electric utilities are investing millions of dollars in systems that enable more precise weather and fire risk forecasting. This capability allows them to monitor challenges posed to their transmission and distribution systems in real-time [15]. With the advent of advanced visualization and monitoring technologies, real-time and proactive operation-oriented measures can effectively be applied to enhance the resilience of the system during extreme events [16].

Among the operational measures to reduce wildfire effects are segmenting distribution systems into networked microgrids [17], routing and scheduling mobile energy sources [18], and managing mobile loads, such as evacuation of electric vehicles during extreme wildfires [19]. In case of a progressing wildfire, dynamic adjustments of line ratings can also provide flexibility as well as ensure optimal and safe utilization of distribution and transmission capacity [20]. During a wildfire, the overhead conductors of a distribution line suffer a thermal stress that deteriorates their mechanical properties [21]. In places with low height combustibles, small and moderate wildfires do not melt the conductors, but cause a thermal stress to the line. Nazemi and Dehghanian [22], Nazemi et al. [23], Trakas and Hatziargyriou [24] utilize the steady-state heat balance equations provided in [25] to improve the resilience of the power distribution systems through mitigation, response, and recovery.

While prior studies have explored the impact of heat gain on conductors and the influence of environmental conditions and line currents on line capacities, they have primarily focused on de-energizing the line when its temperature exceeds the allowable maximum. Subsequently, they determine the optimal power generation from generators and energy storage devices to minimize the need for load shedding. However, it remains crucial to devise strategies that aid in preventing the line temperature from exceeding its maximum thermal capacity.

The research efforts have been focused on preparing the grid for natural disasters or after the disaster occurs; however, the literature has yet to explore deeply the grid management during the course of an event. Donaldson et al. [19] and Abdelmalak and Benidris [26] emphasize the importance of proactive grid preparation, highlighting the critical role of integrating dynamic system constraints and resources to enhance the operational resilience of power systems against wildfires. However, these models are specifically designed for power transmission grids and do not incorporate a detailed wildfire spread model.

Efficiently optimizing distribution grid reconfiguration and power grid capacities is crucial for enhancing operational resilience against natural disasters. In [27], the resilience of distribution grids is enhanced through distributed generation planning and reconfiguration under various fault scenarios. Rostamzadeh et al. [28] develops an outage management approach for power distribution systems, enhancing resilience during outages through efficient deployment of mobile power sources and effective network topology utilization. In [29], Taheri et al. introduce a methodology to enhance power distribution system resilience, incorporating remote-control, manual switches, and distributed generations. Home-Ortiz et al. [30] explore the integration of demand response, network reconfiguration, and the utilization of mobile emergency generation units and solar PV generation. The abovementioned references utilize real-time reconfiguration, illustrating its potential and feasibility in efficiently managing power distribution grids, particularly during the progression of natural disasters.

The primary focus of this article is to develop a dynamic reconfiguration strategy to enhance the operational resilience of power distribution grids against progressive wildfire conditions. During wildfire events, the proposed approach will dynamically adjust line capacities to reduce load curtailments and operational costs. Wildfire impacts on the line conductors are characterized and dynamic line rating constraints are fed into a mixed-integer conic programming reconfiguration model, allowing the feeder to remain energized as long as the temperature of the line conductors is below its maximum allowable limit. Utilizing the CVX environment and MOSEK solver, the optimization model is implemented on two distribution systems: a 33-node network and a practical distribution grid from the Taiwan Power Company (TPC). The evaluation of wildfire scenarios' effects on the distribution grids is conducted. Also, the model is tested when ACSR conductors are replaced with their high-temperature, low-sag counterparts.

This article aims to enhance the grid's flexibility and minimize unnecessary de-energization in the face of small to moderate progressive wildfires. It offers power system operators a proactive strategy that, upon wildfire occurrence, assesses the vulnerability of overhead power distribution lines and determines whether to maintain their energized state as long as thermal stress remains below emergency thresholds.

The contributions of this article are summarized as follows.

1) The real-time reconfiguration of the distribution system is integrated with the dynamic line rating of the overhead lines to enhance distribution grid resilience during progressive wildfires.
2) An integer conic programming model is applied to reduce load curtailment and emergency generator (EG) operation costs.
3) Performance of the model is studied under wildfire-line interaction scenarios as well as under upgrade scenarios of distribution lines with high-temperature, low-sag conductors.

The rest of this article is organized as follows. Section II introduces the wildfire model, including the dynamic thermal rating (DTR) model and the role wildfire plays in raising overhead conductor temperatures. The problem formulation of the proposed framework is presented in Section III. Numerical results are presented in Section IV. Finally, Section V concludes this article.

II. Wildfire-Conductor Model

A. Dynamic Thermal Rating Model

Traditionally, transmission and distribution lines were operated based on static line rating, which represents the maximum amount of current they could carry based on conservative assumptions on environmental conditions [31]. DTR suggests that line capacities are dynamically affected by environmental conditions and line characteristics, allowing the thermal rating to be adjusted accordingly. By introducing flexibility and ensuring optimal and safe utilization of transmission and distribution capacity, DTR is able to handle emergency situations such as unforeseen temperature rise in conductors [31]. There are a number of factors that influence the conductor temperature, including ohmic losses caused by the conductor current and resistance, solar heat gain, convective cooling, and radiation heat loss [25]. The IEEE Standard 738-1993 [25] describes a model that determines the current-temperature relationship for bare overhead conductors

$$RI^2 + \mathcal{H}_s = \mathcal{H}_r + \mathcal{H}_c. \tag{1}$$

The left side of (1) indicates the heat gain from ohmic losses and solar radiation, which increases the conductor's temperature, and the right side represents the radiative and convective heat losses that decrease the conductor's temperature. $\mathcal{H}_s$, $\mathcal{H}_r$, and $\mathcal{H}_c$ are given by the following equations:

$$\mathcal{H}_s = \alpha_{\text{sun}}\, Q_s \sin(\theta_s)\; A' \tag{2}$$

$$\mathcal{H}_r = 17.8 D_c \varepsilon_c \left[\left(\frac{T_c+273}{100}\right)^4 - \left(\frac{T_a+273}{100}\right)^4\right] \tag{3}$$

$$\mathcal{H}_c = \max\Big[k_a K_{\text{angle}}\left(1.01 + 1.35 N_{Re}^{0.52}\right)(T_c - T_a),\; 0.754 k_a K_{\text{angle}} N_{Re}^{0.6}(T_c - T_a),\; 3.645 \rho_a^{0.5} D_c^{0.75} (T_c - T_a)^{1.25}\Big] \tag{4}$$

where $T_c = T_c^{\max}$, and N_{Re} and K_{angle} are given by the following equations:

$$N_{Re} = \frac{D_c \rho_a V_{\text{wind}}}{\mu_a} \tag{5}$$

$$K_{\text{angle}} = 1.194 - \cos(\theta_{\text{wind}}) + 0.194\cos(2\theta_{\text{wind}}) + 0.368\sin(2\theta_{\text{wind}}). \quad (6)$$

$\mathcal{H}_c$ is selected as the largest value among low-speed wind-forced convective heat loss rate, high-speed wind-forced convective heat loss rate, and natural wind-forced convective heat loss rate of conductor.

B. Wildfire Adds to the Heat Gain

The analysis of wildfire behavior can be conducted using theoretical models, empirical models, or semiempirical models. We utilize a theoretical model to ensure the versatility of our approach to diverse geographical locations and scenarios, making it well-suited for a wide range of networks. Theoretical models rely on principles from fluid mechanics, combustion, and heat transfer [32]. Heat transfer mechanisms such as convection and radiation can contribute to the temperature rise of overhead conductors during wildfires. Equation (1) can be rewritten as

$$RI^2 + \mathcal{H}_s + \mathcal{H}_{rf} + \mathcal{H}_{cf} = \mathcal{H}_r + \mathcal{H}_c. \quad (7)$$

Similar to [23] and [24] convective transmission is neglected since it only affects the temperature of the conductors when the fire is exactly under the overhead lines at which point the line is considered to be out of order.

$\mathcal{H}_{rf}$ is defined by

$$\mathcal{H}_{rf} = D_c \varphi_{frr} \quad (8)$$

where the fire radiative heat flux φ_{frr} is calculated by

$$\varphi_{frr} = \tau\varepsilon_{FZ}\partial_B T_f^4 \left[\alpha_{vf}(r_{inf}, \beta_{inf}) + \alpha_{vf}(r_{\text{sup}}, \beta_{\text{sup}})\right]. \quad (9)$$

r_{inf}, β_{inf}, r_{sup}, β_{sup}, α_{vf} are given by the following equations:

$$r_{inf} = \mathfrak{r}_{fr} \quad (10)$$

$$\beta_{inf} = \tan^{-1}\left(\frac{h_L}{r_{\text{inf}} - h_L\tan(\gamma)}\right) \quad (11)$$

$$r_{\text{sup}} = \mathfrak{r}_{fr} - h_L\tan(\gamma) \quad (12)$$

$$\beta_{\text{sup}} = \tan^{-1}\left(\frac{h_L}{r_{\text{sup}} - (L - h_L\tan(\gamma))}\right) \quad (13)$$

$$\alpha_{vf}(r_{fr}, \vartheta_{fr}) = \frac{\tan^{-1}\left(\frac{2r_{fr}\cos(\gamma)\sin(\vartheta_{fr})\sqrt{z}}{\frac{W^2}{4}\cos(2\gamma - \vartheta_{fr}) + z\cos(\vartheta_{fr})}\right)}{\frac{2\pi}{W\cos(\gamma)}\sqrt{z}} - \frac{1}{\pi}\tan^{-1}\left(\frac{\frac{1}{2}W\cos(2\gamma - \vartheta_{\text{fr}})}{r_{\text{fr}}\cos(\gamma)}\right)\sin(\vartheta_{\text{fr}}) \quad (14)$$

where z is given by

$$z = \frac{W^2}{4} + (\mathfrak{r}_{fr}\cos(\gamma))^2. \quad (15)$$

The distance between the fire and the affected line r_{fr} is described as

$$\mathfrak{r}_{fr} = r_{fr}^0 - V_{fr}\,\Delta t\cos(\theta_{\text{wind}}). \quad (16)$$

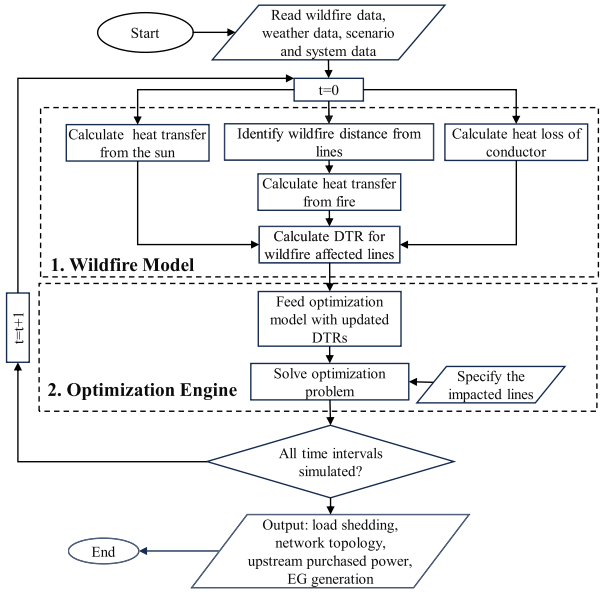

Fig. 1. Big picture of the proposed framework.

Here, V_{fr} is dependent on the wind speed and fuel bulk density as given in

$$V_{fr} = \frac{k(1 + V_{\text{wind}})}{\rho_b} \quad (17)$$

where k is assumed to be 0.07 kg/m3 for wildfire in wildland area.

III. Problem Formulation

In this section, the problem of optimal proactive decision making for power distribution systems [33] facing a progressive wildfire is formulated as a mixed-integer conic programming problem [34]. The wildfire and the DTR models will be used as inputs to the optimization engine. The overall framework of the proposed model is depicted in Fig. 1. Next, we discuss the objective function and constraints.

A. Objective Function

$$\min \sum_{i\in\psi_B}\left(VOLL_i\, x_i\, P_i^D\right) + \sum_{i\in\psi_{EG}}\left(\mathcal{C}_i^{EG}\, P_i^{EG}\right) + \mathcal{C}^{\text{grid}}\, P^{\text{grid}} \quad (18)$$

The objective function (18) includes three terms to be minimized. The first term represents the cost of load shedding during a progressive wildfire. The assessment of the criticality of various loads in power systems is aided by the concept of the value of the lost load (VoLL). VoLL is the cost that customers of the power system incur when there is an interruption in electricity service. Priority will be given to loads with higher VoLL to remain energized. The second term is the generation costs of EG, which could be expensive, depending on the availability of diesel. The third term calculates the cost of power purchased from the upstream network. In (18), x_i is used as a continuous variable

representing the percentage of curtailed load at node i. The cost associated with load shedding is calculated by multiplying the VoLL by the quantity of curtailed load at each individual node. Constraints on the objective function (18) include the following.

B. Constraints

1) Power Flow Equations: Active and reactive power balance equations are as follows:

$$\sum_{j\in\mathcal{N}(i)} \mathcal{Y}_{ij}\, P_{ij} = P_i^{EG} - (1-x_i)\; P_i^D, \quad i\in\psi_B \tag{19}$$

$$\sum_{j\in\mathcal{N}(i)} \mathcal{Y}_{ij}\, Q_{ij} = Q_i^{EG} - (1-x_i)\; Q_i^D, \quad i\in\psi_B. \tag{20}$$

P_{ij} and Q_{ij} are given by

$$P_{ij} = g_{ij}\, V_i^2 - V_i V_j\, (g_{ij}\cos\theta_{ij} + b_{ij}\sin\theta_{ij}) \tag{21}$$

$$Q_{ij} = V_i\, V_j\, (b_{ij}\cos\theta_{ij} - g_{ij}\sin\theta_{ij}) - \left(b_{ij} + \frac{b_{ij}^{sh}}{2}\right) V_i^2. \tag{22}$$

$\theta_{ij} = \theta_i - \theta_j$ is the node voltage angle difference between nod i and j.

Node voltage and line current capacity are described by the following constraints:

$$\underline{V_i} \le V_i \le \overline{V_i},\; i\in\psi_B \tag{23}$$

$$I_{ij}^2 \le \bar{I}_{ij}^2 \tag{24}$$

and

$$I_{ij}^2 = \mathcal{Y}_{ij}\left(\mathcal{A}_{ij}V_i^2 + \mathcal{B}_{ij}V_j^2 - 2V_iV_j\,(\mathcal{C}_{ij}\cos\theta_{ij} - \mathcal{D}_{ij}\sin\theta_{ij})\right), \quad ij\in\psi_L \tag{25}$$

where

$$\mathcal{A}_{ij} = g_{ij}^2 + \left(b_{ij} + \frac{b_{ij}^{sh}}{2}\right)^2 \tag{26}$$

$$\mathcal{B}_{ij} = g_{ij}^2 + b_{ij}^2 \tag{27}$$

$$\mathcal{C}_{ij} = g_{ij}^2 + b_{ij}\left(b_{ij} + \frac{b_{ij}^{sh}}{2}\right) \tag{28}$$

$$\mathcal{D}_{ij} = \frac{g_{ij}\, b_{ij}^{sh}}{2}. \tag{29}$$

Power flow equations include a set of nonconvex constraints. With the help of auxiliary variables, we can formulate the problem as a convex second-order cone program. According to [34], we define two new auxiliary variables $\mathcal{R}_{ij}$ and $\mathcal{T}_{ij}$ for each line and $\mathcal{V}_i$ for each node as follows:

$$\mathcal{V}_i = \frac{V_i^2}{\sqrt{2}}\; i\in\; \psi_B \tag{30}$$

$$\mathcal{R}_{ij} = V_i\, V_j\, \cos\theta_{ij}\; ij\in\psi_L \tag{31}$$

$$\mathcal{T}_{ij} = V_i\, V_j\, \sin\theta_{ij}\; ij\in\psi_L. \tag{32}$$

Given (30)–(32), (21)–(23) can be rewritten as follows:

$$P_{ij} = \sqrt{2}\, g_{ij}\mathcal{V}_i - g_{ij}\mathcal{R}_{ij} - b_{ij}\mathcal{T}_{ij} \tag{33}$$

$$Q_{ij} = -\sqrt{2}\left(b_{ij} + \frac{b_{ij}^{sh}}{2}\right)\mathcal{V}_i + b_{ij}\mathcal{R}_{ij} - g_{ij}\mathcal{T}_{ij} \tag{34}$$

$$\frac{\underline{V_i}^2}{\sqrt{2}} \le \mathcal{V}_i \le \frac{\overline{V_i}^2}{\sqrt{2}}. \tag{35}$$

Equations (31) and (32) can be integrated into one constraint as given as

$$2\mathcal{V}_i\,\mathcal{V}_j = \mathcal{R}_{ij}^2 + \mathcal{T}_{ij}^2,\; \mathcal{R}_{ij}\ge 0\,. \tag{36}$$

However, (36) is a nonlinear equation and according to [33] needs to be relaxed as a convex rotated conic inequality constraint:

$$2\mathcal{V}_i\mathcal{V}_j \ge \mathcal{R}_{ij}^2 + \mathcal{T}_{ij}^2,\; \mathcal{R}_{ij}\ge 0\,. \tag{37}$$

In order to consider the reconfiguration of the network to increase the network's resiliency against the approaching wildfire, we must define two new auxiliary variables for each line ij, $\mathcal{V}_i^{ij}$ and $\mathcal{V}_j^{ij}$. It is important to note that if the line is disconnected ($\mathcal{Y}_{ij} = 0$), the new variables will be equal to zero, and if the line is connected ($\mathcal{Y}_{ij} = 1$), the new variables will take the following values:

$$\mathcal{V}_i^{ij} = \frac{V_i^2}{\sqrt{2}} \quad \mathcal{V}_j^{ij} = \frac{V_j^2}{\sqrt{2}}. \tag{38}$$

Using the auxiliary variables for nodes and lines, we can write

$$0 \le \mathcal{V}_i^{ij} \le \frac{\bar{V}_i^2}{\sqrt{2}}\mathcal{Y}_{ij} \qquad ij\in\psi_L \tag{39}$$

$$0 \le \mathcal{V}_j^{ij} \le \frac{\bar{V}_j^2}{\sqrt{2}}\mathcal{Y}_{ij} \qquad ij\in\psi_L \tag{40}$$

$$0 \le \mathcal{V}_i - \mathcal{V}_i^{ij} \le \frac{\bar{V}_i^2}{\sqrt{2}}(1-\mathcal{Y}_{ij}) \qquad ij\in\psi_L \tag{41}$$

$$0 \le \mathcal{V}_j - \mathcal{V}_j^{ij} \le \frac{\bar{V}_j^2}{\sqrt{2}}(1-\mathcal{Y}_{ij}) \qquad ij\in\psi_L \tag{42}$$

$$P_{ij} = \sqrt{2}\, g_{ij}\mathcal{V}_i^{ij} - g_{ij}\mathcal{R}_{ij} - b_{ij}\mathcal{T}_{ij} \qquad ij\in\psi_L \tag{43}$$

$$Q_{ij} = -\sqrt{2}\left(b_{ij} + \frac{b_{ij}^{sh}}{2}\right)\mathcal{V}_i^{ij} + b_{ij}\mathcal{R}_{ij} - g_{ij}\mathcal{T}_{ij} \qquad ij\in\psi_L \tag{44}$$

$$2\mathcal{V}_i^{ij}\mathcal{V}_j^{ij} \ge \mathcal{R}_{ij}^2 + \mathcal{T}_{ij}^2,\; \mathcal{R}_{ij}\ge 0,\; ij\in\psi_L \tag{45}$$

$$I_{ij}^2 = \sqrt{2}\mathcal{A}_{ij}\mathcal{V}_i^{ij} + \sqrt{2}\,\mathcal{B}_{ij}\mathcal{V}_j^{ij} - 2\mathcal{C}_{ij}\mathcal{R}_{ij} + 2\mathcal{D}_{ij}\mathcal{T}_{ij}\;,\; ij\in\psi_L. \tag{46}$$

Equations (43)–(44) and (46) give the active power flow, reactive power flow, and line current flowing through line ij. If line ij is disconnected ($\mathcal{Y}_{ij} = 0$), (45) will give $\mathcal{R}_{ij} = \mathcal{T}_{ij} = 0$, resulting in line current, and active and reactive power flows in the line ij equal to zero.

2) Radiality: For the distribution network configurations to be radial, the following constraints [34] must be met:

$$\lambda_{ij} + \lambda_{ji} = \mathcal{Y}_{ij} \quad ij \in \psi_L \tag{47}$$

$$\sum_{j \in \mathcal{N}(i)} \lambda_{ij} = 1 \; i \in \psi_B \tag{48}$$

$$\lambda_{0j} = 0 \; j \in \mathcal{N}_0 \tag{49}$$

$$0 \leq \mathcal{Y}_{ij} \leq 1. \tag{50}$$

Equation (47) indicates that a line between node i and node j is in the spanning tree $\mathcal{Y}_{ij} = 1$ if either node j is the parent of node i (λ_{ij}= 1), or node i is the parent of node j (λ_{ji}= 1). Equation (48) indicates every node except the substation node has exactly one parent, and (49) indicates that the substation node has no parents. $\mathcal{N}(i)$ and $\mathcal{N}_0$ are set of branches connected to node i and set of branches connected to substation node, respectively.

3) EG Operation: Maximum and minimum power generations of EGs are as follows:

$$0 \leq P_i^{\mathrm{EG}} \leq \bar{P}i^{\mathrm{EG}} i \in \Psi_{\mathrm{EG}} \tag{51}$$

$$0 \leq Q_i^{\mathrm{EG}} \leq \bar{Q}i^{\mathrm{EG}} i \in \Psi_{\mathrm{EG}}. \tag{52}$$

$\bar{P}_i^{\mathrm{EG}}$and $\bar{Q}_i^{\mathrm{EG}}$ are maximum active and reactive power generation of EGs at node i, respectively.

Using wildfire scenarios as inputs, this mixed-integer conic model can be solved with commercial solvers and enhance the resilience and proactive operation of distribution systems against progressive wildfires.

IV. Numerical Studies

In this section, we validate the performance of the proposed model by applying it to a modified 33-node network [35] and the 83-node TPC's practical distribution grid [36]. The model was implemented using CVX optimization modeling environment [37] on a desktop computer with Intel Core i7 2.8 GHz and 16 GB RAM. The mixed integer conic optimization problem was solved using MOSEK. The minimum and maximum allowable voltages at each node are considered to be 0.9 and 1.1 p.u., respectively. EGs are operated at 120 $/MWh and the price of energy from upstream is 80 $/MWh. The ACSR conductor type is considered here, which is commonly used for overhead power transmission and distribution lines [20].

The wildfire data and weather parameters are provided in [20] and [38]. It is assumed that the progression of the fire is monitored every ten minutes. This time step was found to be appropriate for modeling DTR based on the change in conductor temperature. Determining VoLL requires extensive data collection. We choose VoLLs for each bus to be between 1000 to 10 000 $/MWh to prioritize the critical loads [22]. This range is indicative of both residential and commercial load characteristics [39]. Since the distribution system covers a small geographic area, its components are expected to experience similar weather conditions.

TABLE I
Specifications for Three Scenarios

Scenario	I	II	III
V_{wind} (m/s)	0.6	0.7	0.8
θ_{wind} (rad)	1	0.8	0.5
Q_s (W/m^2)	1000	900	800
T_a(°C)	40	35	30

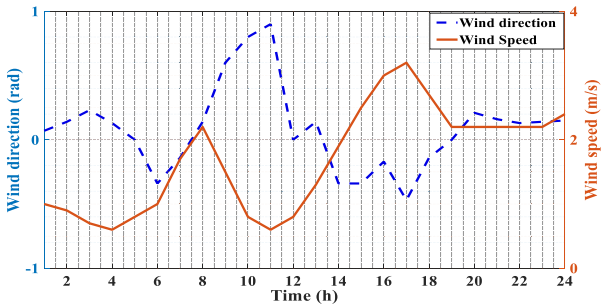

Fig. 2. Wind speed and wind direction for a typical summer day.

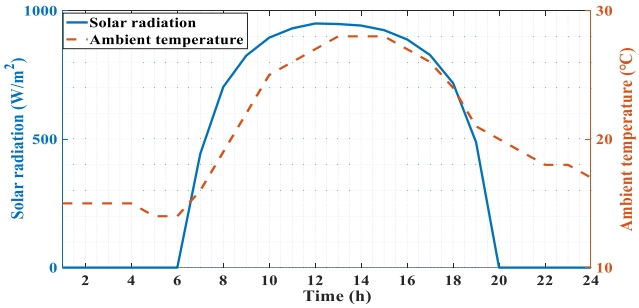

Fig. 3. Solar radiation and ambient temperature for a typical summer day.

A. Impact of Wildfire Progression on DTR

To investigate the wildfire's progression and its impact on the DTR, we analyze four scenarios. Table I gives the specifications for three scenarios, each with fixed values for V_{wind}, θ_{wind}, Q_s, and T_a. The spread of fire is determined by the quantities of wind speed and wind angle, as indicated in (16) and (17). Radiative heat on the conductor surface is also affected by the values of solar heat flux intensity and ambient temperature as shown in (7). The spread and impact of progressive wildfires may therefore differ from one scenario to another. The fourth scenario utilizes real-world data [40], as illustrated in Figs. 2 and 3.

Fig. 4 shows the distance between the fire and distribution line in each scenario. The distance between fire and the conductor is calculated by (16). Starting at 40 m, wildfire approaches the line from different directions at different speeds. In the fourth scenario, we assumed that the fire is 40 m away from the line at the ninth hour.

In the event that a wildfire progresses towards a distribution line, the radiative heat transferred from the fire will affect the line's thermal rating depending on the distance from the line to the fire as shown in Fig. 5. A comparison of the fire behavior in the four scenarios reveals that the line ampacity decreases faster when the wildfire approaches the line more quickly. At the 40-m

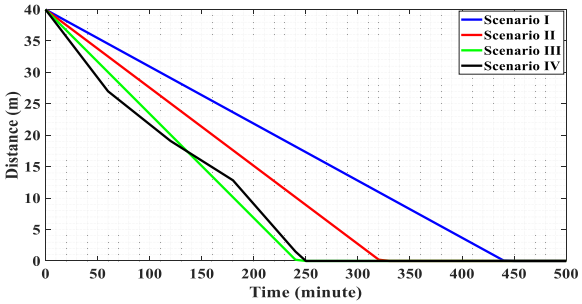

Fig. 4. Different scenarios of the distance between a fire and an affected line.

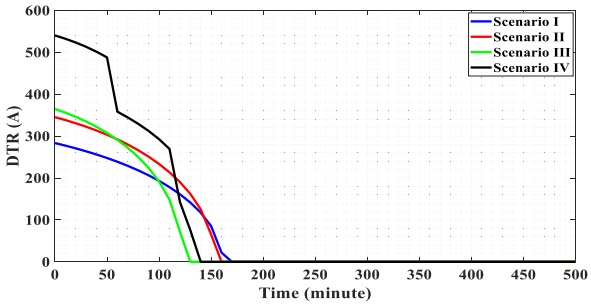

Fig. 5. DTR of an affected line for different scenarios.

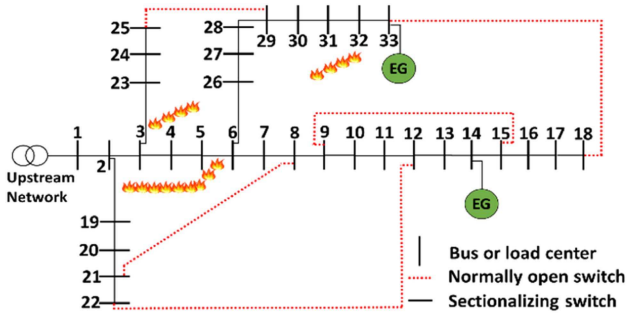

Fig. 6. Modified 33-node test system.

distance, the conductor DTR equals 283, 345, 364, and 540 for scenarios I, II, III, and IV, respectively. The notable change in the curve's slope in the fourth scenario signifies a change in the input weather data. The variation is observed hourly due to the time series data for the real-world scenario being provided with a 1-h resolution.

B. *Modified 33-Node Test System*

Fig. 6 shows the single-line diagram of a modified 33-node feeder, and the data for it can be found in [35]. We assume that the system is balanced with a total active load of 7.43 MW and a total reactive load of 4.6 MVar. In nodes 14 and 33, two EGs with a maximum capacity of 1 MW are available. A topology change can be made by closing or opening five normally open switches and normally closed switches (sectionalizing switches) on the line segments.

1) Effectiveness of the Proposed Model With and Without Reconfiguration: In order to show the effectiveness of the proposed model when a wildfire approaches the distribution line, three line-wildfire interaction cases were studied for each scenario. The case information is given in Table II.

TABLE II
THREE AFFECTED LINE CASES

Cases	Affected lines
I	Line between nodes 2–3
II	Lines between nodes 3–4, and 32–33
III	Lines between nodes 5–6, 2–19, and 3–23

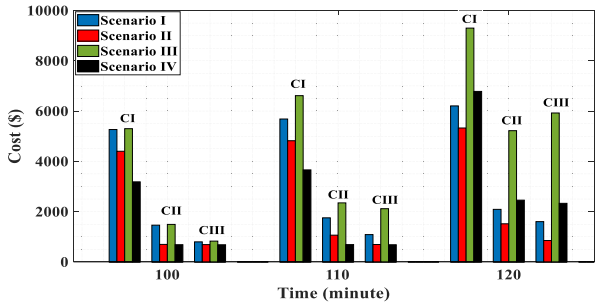

Fig. 7. Objective function value for the scenarios and cases presented in Tables I and II without reconfiguration (CI-III: Case I-III).

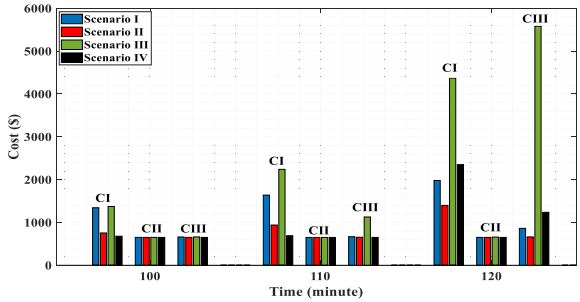

Fig. 8. Objective function value for the scenarios and cases presented in Tables I and II with reconfiguration (CI-III: Case I-III).

The distribution system operation is optimized to minimize the operation costs with and without reconfiguration as wildfire approaches lines. Examining various cases and scenarios, we will demonstrate how operation costs depend on affected lines and input parameters. Fig. 7 presents the objective function values assuming a fixed topology for the grid. Comparing the value of objective functions reveals that the cost in all the three cases increases as the wildfire approaches the distribution line. In the without reconfiguration scenario, even though in case I, only one line is affected, because of the closer location of the line to the substation and the higher flow of current, the reduction in DTR results in higher cost.

Fig. 8 shows that the overall cost of operating the distribution grid under the progressive wildfire is significantly reduced with the help of reconfiguration. One can see that scenario III gives higher cost, and that is because of its lower DTR and higher rate of spread.

Fig. 9 depicts the load shedding at each node during the progress of the wildfire for case I, scenario IV.

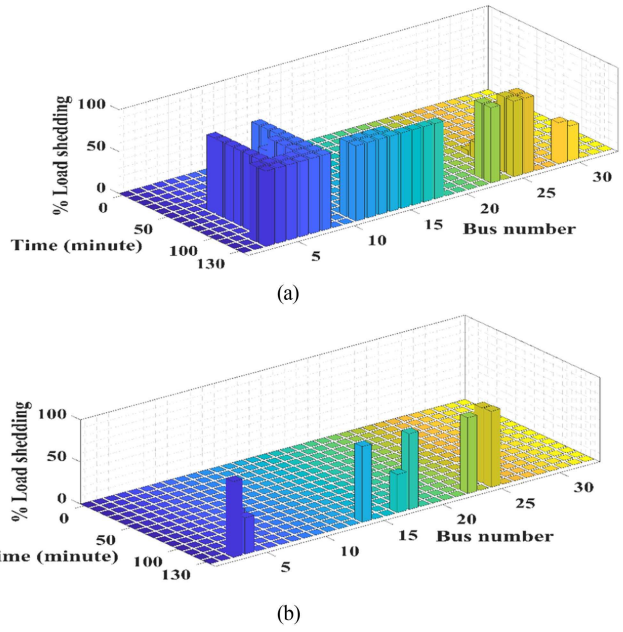

Fig. 9. Load shedding for all nodes during wildfire approaching for: (a) case I, scenario IV, without reconfiguration and (b) case I, scenario IV, with reconfiguration.

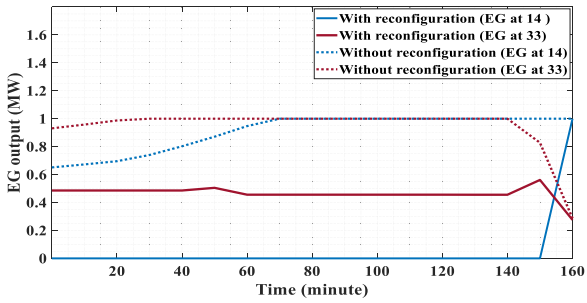

Fig. 10. Generated power of EGs at nodes 14 and 33 for case II, scenario I.

Comparing (a) and (b), one can see the difference between load shedding with and without reconfiguration. Maximum VoLLs have been considered for load points 9, 10, 24, and 27, and, as it can be seen, none of them have been shed. It can also be observed that reconfiguration postpones load shedding which will improve the resilience during the approaching wildfire. Under case I and scenario IV, in the final time interval before the line being considered as out of service, the unserved load in the absence of reconfiguration amounts to 3.72 MW. However, in the case of reconfiguration, the curtailed load is reduced to 1.7 MW. This reduction represents a substantial improvement in the grid's resilience when dealing with a wildfire, and it can serve as a resilience index for electric utilities. Case II is then selected to assess the performance of EGs as this case involves a line that is connected to one of the EGs. Fig. 10 depicts the outputs of EGs as the wildfire approaches the distribution line in scenario I, both with and without reconfiguration. One can see that in the with reconfiguration case, the EGs, except for the one at node 14 during the last time interval, are not being

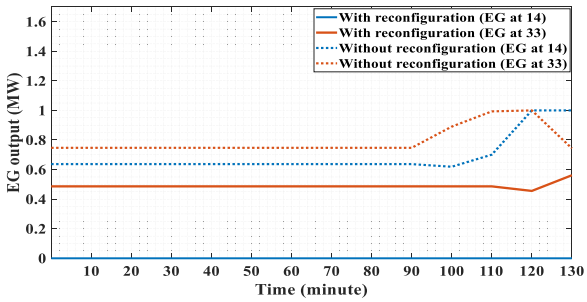

Fig. 11. Generated power of EGs at nodes 14 and 33 for case II, scenario IV.

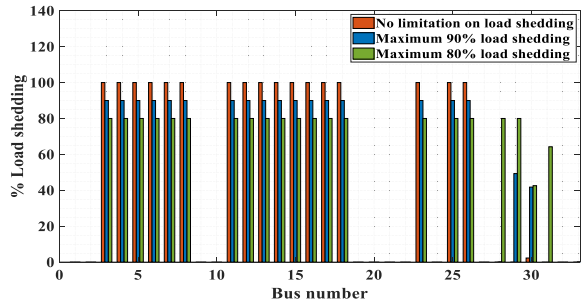

Fig. 12. Percentage of load shedding at each node for case I, scenario IV.

utilized to their maximum capacity. This is because of the higher diesel cost of generators compared to the cost of energy from the upstream grid. It can also be observed that as the impact of fire on line 32–33 becomes more significant, the output of EG at node 33 has to drop to ensure an acceptable maximum thermal rating.

Fig. 11 shows the outputs of EGs for case II, scenario IV. As observed, in the case with reconfiguration, none of the EGs operate at their maximum capacity. Additionally, it was noted that the EG at node 14 remained inactive for the entire time.

2) Investigating the Effect of Maximum Allowable Load Shedding: Here, we investigate a situation where a percentage of loads cannot be shed, and complete load curtailment of 100% is not permitted. This limitation arises from practical constraints experienced by the electric utilities, as they may be unable to curtail the entire load at specific nodes. Some nodes may include medically vulnerable loads [28], and de-energization could potentially pose life-threatening risks to individuals. Fig. 12 provides a comparison of three conditions for case I, scenario IV. This comparison is conducted for the 130-min period following the fire's ignition at a distance of 40 m from the line. The results indicate that the optimization algorithm will shed loads with higher VoLLs to guarantee the minimum supply requirement. For instance, load points 9, 10, 24, and 27 have been designated with a VoLL of 10 000, while load points 28 to 33 belong to the second priority group with a VoLL of 7500. As observed, the algorithm progressively sheds loads from the second priority group as the maximum allowable curtailment limit is raised.

Fig. 13 depicts the changes in the objective function across the three specified maximum curtailment limits for case I, scenario IV. Generally, the cost rises as the wildfire approaches the line.

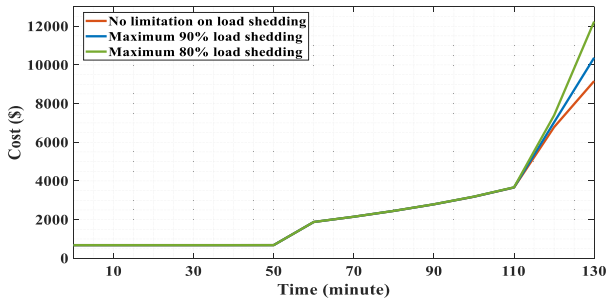

Fig. 13. Operational cost incurred due to an approaching wildfire for case I, Scenario IV.

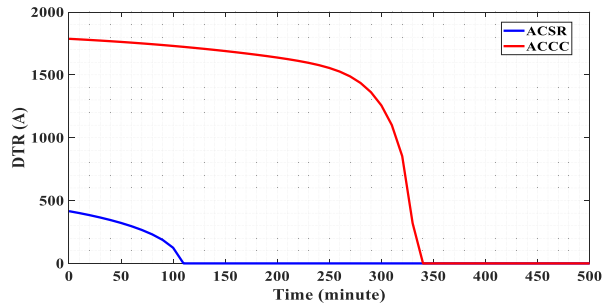

Fig. 14. ACCC and ACSR DTRs for scenario I.

Nevertheless, when we enforce the load curtailment limit, the algorithm must curtail loads with higher VoLLs to maintain the minimum supply requirement. After the 110-minute mark, the steeper curve indicates increased curtailment of higher VoLL loads.

3) Investigating the Effect of High-Temperature, Low-Sag Conductors: Wildfires affect conductors differently depending on their type. A high-temperature, low-sag conductor could potentially replace ACSR conductors in wildfire-prone areas [41].

ACCC conductors are designed to maintain the same overall diameter as a conventional round wire ACSR; however, they double the current carrying capacity over conventional ACSR [42]. This can allow utility to reconductor existing pathways without structural modification. They can be operated to 180 °C versus the existing ACSR with its conventional 75 °C limit. In this section, we investigate the impact of line conductor characteristics on the objective function. Two conductors are considered as follows.

1) *Conductor Type 1:* ACSR 795, 26/7 with the ampacity of 907 A, the diameter of 1.1 inches, and resistance of 0.026 Ω/kft.
2) *Conductor Type 2:* ACCC 1026 with the ampacity of 1770 A, the diameter of 1.1 inches, and resistance of 0.0205 Ω/kft.

To better compare the impact of wildfires on the conductors, we multiply the total load of the grid by a factor of 1.5. Fig. 14 shows the difference between the DTRs of the two conductors for scenario I. As it can be seen, the DTR curve for the ACCC conductor is considerably higher than that of ACSR.

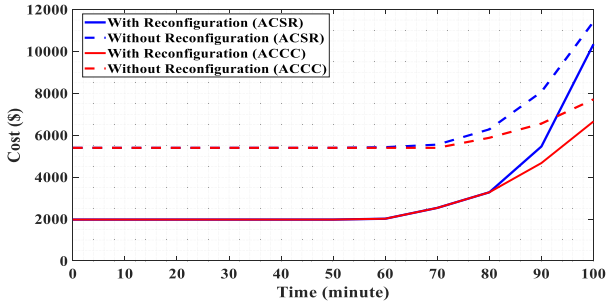

Fig. 15. Objective function values for ACCC and ACSR conductors in line between nodes 5 and 6, with and without reconfirmation.

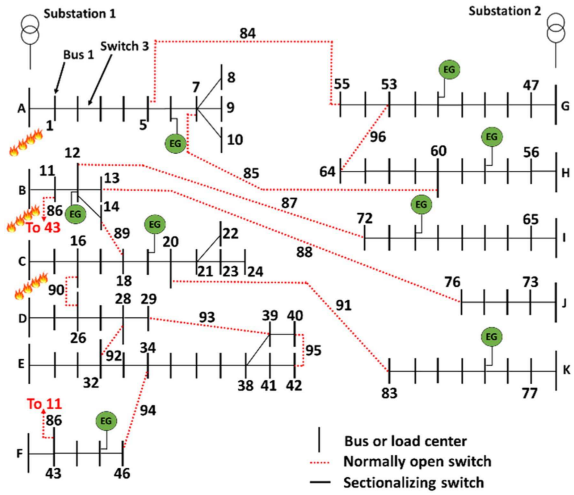

Fig. 16. Practical TPC's distribution network.

To demonstrate the impact of the ACCC conductor on the objective function, we consider case III and run the optimization model assuming the type 1 and type 2 conductors for the line between nodes 5 and 6. Due to the fact that the line between nodes 5 and 6 serves a substantial amount of load in the feeder, the conductor of this line has been upgraded. The values of the objective function are shown in Fig. 15.

The comparison shows that the cost significantly drops when ACCC conductor is installed. As it can be seen, before time equals to 90 min, ACCC without reconfiguration has a higher cost than ACSR with reconfiguration.

C. Investigating the Effect of Larger Distribution Network With Two Substations

The accuracy of the proposed approach is further demonstrated using the TPC's practical distribution network, which consists of 83 nodes and operates at 11.4 kV. This network includes two substations, 11 feeders, 83 normally closed switches, and 13 normally open switches [36]. It is assumed that the system is balanced with a constant load. The single-line diagram of the test system is presented in Fig. 16. For this article, the network was modified by integrating eight EGs, each with a maximum capacity of 1 MW. In order to show the effectiveness of the proposed model when a wildfire approaches the distribution line,

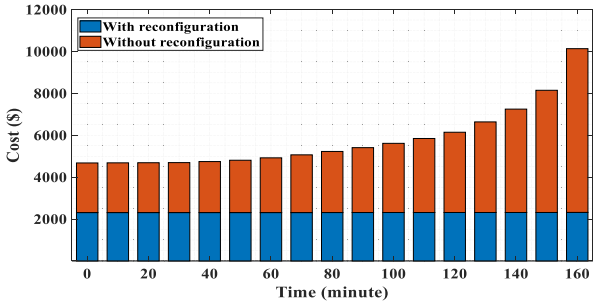

Fig. 17. Objective function value for TPC network with and without reconfiguration for scenario I.

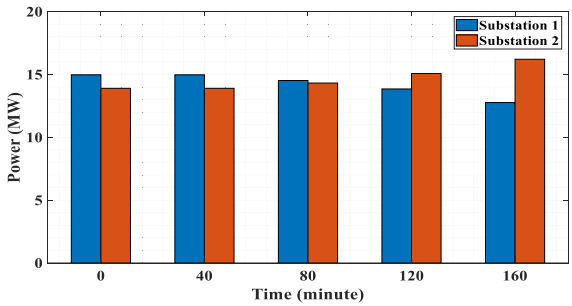

Fig. 18. Power supplied by each substation during the approaching wildfire for the TPC network with reconfiguration.

it is assumed that the feeders A, B, and C are affected by wildfire. Fig. 17 illustrates a comparison between the objective functions of the TPC's network with and without reconfiguration. The results indicate that with a fixed grid topology, the cost increases as the wildfire approaches the feeders. The increase in cost is attributed to both the expenses associated with shedding loads and the generation of EGs. As the fire approaches the line, the DTR decreases, resulting in load curtailment. However, reconfiguration will enable the supply of the affected load on feeders A, B, and C to be routed through alternative feeders. This has been demonstrated with a nearly consistent cost in the case with reconfiguration. We chose scenario I here because it exhibits the slowest fire spread among the four scenarios.

Fig. 18 demonstrates the impact of wildfire on the power supplied by each substation. By comparing the power supplied during different time intervals, it becomes evident that when the wildfire is sufficiently distant and has a minor effect on the feeders, substation 1 supplies a larger portion of the load. However, as the wildfire approaches the feeders, the DTR of feeders A, B, and C decreases, leading to a reduction in the power supplied by substation 1. This illustrates how wildfires can alter the way power is distributed among substations and potentially increase the load on transformers.

A comparison between with and without reconfiguration for the TPC grid under scenario I shows a significant drop in the amount of unserved load from 5.87 to 0 MW, in the final time interval before the line being considered as out of service. This reduction represents a substantial improvement in the TPC grid's resilience.

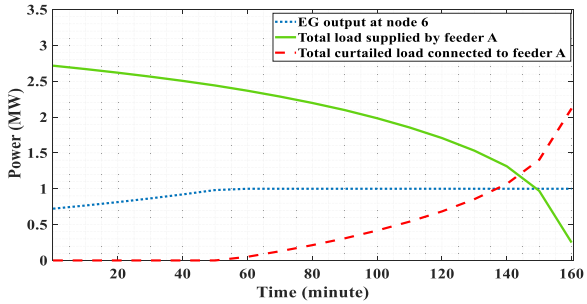

Fig. 19. EG power production, load shedding, and power flow along feeder A during the approaching wildfire for the TPC network without reconfiguration.

Fig. 19 depicts how the EG power production, amount of curtailed load connected to feeder A, and power supplied to this feeder changes when the wildfire approaches the TPC network and network reconfiguration is not allowed. Initially, a large portion of the load is supplied by feeder A. However, as wildfire gets closer, EG power production increases, avoiding the need for load shedding. When EG reaches its maximum power capacity and feeder A cannot supply load due to the reduction in its DTR, the load starts to shed. As the fire nears feeder A, a greater portion of the total load connected to feeder A is shed. With reconfiguration, there is no shedding of any load connected to this feeder.

The results from the two networks underscore the critical role that reconfiguration could potentially play in sustaining grid operation and supplying power to more loads during the advancement of small to moderate wildfires. This has the potential to offer substantial benefits to electric utilities, enhancing system reliability, resilience, reducing outage durations, avoiding unnecessary power shutdowns, and minimizing economic losses during wildfire events. This gains greater significance as wildfires continue to expand and are expected to grow in the near future.

V. Conclusion and Future Work

This article presents a proactive decision-making framework for determining the optimal topology of the power distribution grids facing a progressive wildfire. The framework is modeled as a mixed-integer conic programming problem, where heat balance equations are used to analyze the effects of wildfires on overhead line thermal ratings. Through dynamically rating distribution lines and reconfiguring the grid, as well as controlling the flow of current through distribution lines, the amount of curtailed loads is minimized and line sags are avoided. Numerical results show that the proposed optimization framework can economically enhance the resilience of the distribution grid and ensure load connectivity under progressive wildfires. Some of the key findings of are as follows: DTR is influenced by weather data and the distance of the fire from the line. Furthermore, it can be seen that the location of affected lines within the feeder plays a crucial role in determining the impact of wildfires on load shedding and associated costs. The results also demonstrate that the decrease in the current limit of the lines due to wildfires can impact the utilization of EGs during

emergency conditions. It is important to note that lines with greater temperature resistance enhance the grid's capability to provide power to a higher number of loads during wildfire events. It was also observed that in power distribution grids with two substations, reconfiguration can offer increased flexibility, thereby enhancing the system's resilience when facing an approaching wildfire. In summary, the results suggest that the proposed model can provide electric utility operators with both extra time and a safety buffer before making the decision to de-energize the grid when dealing with small to moderate wildfires.

Future work will include the development of a comprehensive optimization model for both distribution systems hardening and reconfiguration to enhance the resilience of the grid against progressive wildfires. A potential avenue for future research could involve the co-optimization of monitoring and actuation devices together with the reconfiguration problem. Another promising area for future research could be the integration of theoretical and empirical models to improve the prediction of the progression of smaller wildfires. As more data becomes accessible, this approach could significantly enhance the decision-making capabilities of electric utilities when dealing with wildfires. By combining the theoretical and empirical models, it becomes possible to address some of the limitations of the theoretical model, such as the inclusion of additional attributes like detailed land cover characteristics.

REFERENCES

[1] J. Wang and K. Strong, "British Columbia's forest fires, 2018," Dec. 17, 2022, [Online]. Available: https://www150.statcan.gc.ca/n1/en/pub/16-508-x/16-508-x2019002-eng.pdf?st=VZhcBQZe

[2] A. I. Filkov, T. Ngo, S. Matthews, S. Telfer, and T. D. Penman, "Impact of Australia's catastrophic 2019/20 bushfire season on communities and environment. Retrospective analysis and current trends," *J. Saf. Sci. Resilience*, vol. 1, no. 1, pp. 44–56, 2020.

[3] D. A. Z. Vazquez, F. Qiu, N. Fan, and K. Sharp, "Wildfire mitigation Plans in power systems: A literature review," *IEEE Trans. Power Syst.*, vol. 37, no. 5, pp. 3540–3551, Sep. 2022, doi: 10.1109/TPWRS.2022.3142086.

[4] NOAA National Centers for Environmental Information, "Monthly wildfires report for annual 2021," Jan. 2022. Accessed: Dec. 12, 2023. [Online]. Available: https://www.ncei.noaa.gov/access/monitoring/monthly-report/fire/202113

[5] T. Sanford, R. Wang, and A. Kenward, "The age of Alaskan wildfires," in *Climate Central*. Princeton, NJ, USA, 2015.

[6] U.S. Department of Agriculture (USDA), "The rising cost of fire operations: Effects on the forest service's non-fire work," US Dept. Agriculture Forest Service, Washington, DC, USA, 2015.

[7] D. Thomas, D. Butry, S. Gilbert, D. Webb, and J. Fung, "The Costs and losses of wildfires: A literature review," NIST Special Publication 1215, U.S. Department of Commerce, 2017. [Online]. Available: https://nvlpubs.nist.gov/

[8] N. Rhodes, L. Ntaimo, and L. Roald, "Balancing wildfire risk and power outages through optimized power shut-offs," *IEEE Trans. Power Syst.*, vol. 36, no. 4, pp. 3118–3128, Jul. 2021, doi: 10.1109/TPWRS.2020.3046796.

[9] C. Proctor, A. Whelton, A. Shah, and J. Lee, "Fire and water," *Civil Eng. Mag. Arch.*, vol. 91, no. 1, pp. 42–47, 2021.

[10] S. Anderson, C. Barford, and P. Barford, "Five alarms: Assessing the vulnerability of us cellular communication infrastructure to wildfires," in *Proc. ACM Internet Meas. Conf. Ser.*, 2020, pp. 162–175.

[11] J. W. Muhs, M. Parvania, H. T. Nguyen, and J. A. Palmer, "Characterizing probability of wildfire ignition caused by power distribution lines," *IEEE Trans. Power Del.*, vol. 36, no. 6, pp. 3681–3688, Dec. 2021, doi: 10.1109/TPWRD.2020.3047101.

[12] S. Tandon, S. Grijalva, and D. K. Molzahn, "Motivating the use of dynamic line ratings to mitigate the risk of wildfire ignition," in *Proc. IEEE Power Energy Conf. Illinois*, 2021, pp. 1–7, doi: 10.1109/PECI51586.2021.9435252.

[13] S. Ma, B. Chen, and Z. Wang, "Resilience enhancement strategy for distribution systems under extreme weather events," *IEEE Trans. Smart Grid*, vol. 9, no. 2, pp. 1442–1451, Mar. 2018, doi: 10.1109/TSG.2016.2591885.

[14] S. Hojjatinejad and M. Ghassemi, "Resiliency enhancement against wildfires," in *Proc. IEEE Power Energy Soc. Innov. Smart Grid Technol. Conf.*, 2021, pp. 1–5, doi: 10.1109/ISGT49243.2021.9372206.

[15] T. Sickinger, "Oregon utilities to use AI, data to predict wildfire threat," Jun. 2022, [Online]. Available: https://www.govtech.com/products/oregon-utilities-to-use-ai-data-to-predict-wildfire-threat

[16] M. H. Amirioun, F. Aminifar, and H. Lesani, "Resilience-oriented proactive management of microgrids against windstorms," *IEEE Trans. Power Syst.*, vol. 33, no. 4, pp. 4275–4284, Jul. 2018, doi: 10.1109/TPWRS.2017.2765600.

[17] Z. Wang and J. Wang, "Self-healing resilient distribution systems based on sectionalization into microgrids," *IEEE Trans. Power Syst.*, vol. 30, no. 6, pp. 3139–3149, Nov. 2015, doi: 10.1109/TPWRS.2015.2389753.

[18] S. Lei, C. Chen, H. Zhou, and Y. Hou, "Routing and scheduling of mobile power sources for distribution system resilience enhancement," *IEEE Trans. Smart Grid*, vol. 10, no. 5, pp. 5650–5662, Sep. 2019, doi: 10.1109/TSG.2018.2889347.

[19] D. L. Donaldson, M. S. Alvarez-Alvarado, and D. Jayaweera, "Integration of electric vehicle evacuation in power system resilience assessment," *IEEE Trans. Power Syst.*, vol. 38, no. 4, pp. 3085–3096, Jul. 2023, doi: 10.1109/TPWRS.2022.3206900.

[20] M. Choobineh, B. Ansari, and S. Mohagheghi, "Vulnerability assessment of the power grid against progressing wildfires," *Fire Saf. J.*, vol. 73, pp. 20–28, 2015.

[21] E. I. Koufakis, P. T. Tsarabaris, J. S. Katsanis, C. G. Karagiannopoulos, and P. D. Bourkas, "A wildfire model for the estimation of the temperature rise of an overhead line conductor," *IEEE Trans. Power Del.*, vol. 25, no. 2, pp. 1077–1082, Apr. 2010, doi: 10.1109/TPWRD.2009.2035128.

[22] M. Nazemi and P. Dehghanian, "Powering through wildfires: An integrated solution for enhanced safety and resilience in power grids," *IEEE Trans. Ind. Appl.*, vol. 58, no. 3, pp. 4192–4202, May/Jun. 2022, doi: 10.1109/TIA.2022.3160421.

[23] M. Nazemi, P. Dehghanian, M. Alhazmi, and Y. Darestani, "Resilience enhancement of electric power distribution grids against wildfires," in *Proc. IEEE Ind. Appl. Soc. Annu. Meeting*, 2021, pp. 1–7, doi: 10.1109/IAS48185.2021.9677372.

[24] D. N. Trakas and N. D. Hatziargyriou, "Optimal distribution system operation for enhancing resilience against wildfires," *IEEE Trans. Power Syst.*, vol. 33, no. 2, pp. 2260–2271, Mar. 2018, doi: 10.1109/TPWRS.2017.2733224.

[25] *IEEE Standard for Calculating the Current-Temperature Relationship of Bare Overhead Conductors*, IEEE Std 738-2012 (Revision of IEEE Std 738-2006 - Incorporates IEEE Std 738-2012 Cor 1-2013), Dec. 23, 2013.

[26] M. Abdelmalak and M. Benidris, "Enhancing power system operational resilience against wildfires," *IEEE Trans. Ind. Appl.*, vol. 58, no. 2, pp. 1611–1621, Mar./Apr. 2022, doi: 10.1109/TIA.2022.3145765.

[27] H. Wang, S. Wang, L. Yu, and P. Hu, "A novel planning-attack-reconfiguration method for enhancing resilience of distribution systems considering the whole process of resiliency," *Int. Trans. Elect. Energy Syst.*, vol. 30, no. 2, Feb. 2020, Art. no. 12199.

[28] M. Rostamzadeh, M. H. Kapourchali, L. Zhao, and V. Aravinthan, "Outage management of power distribution systems with electricity-dependent medically-vulnerable critical loads," in *Proc. IEEE/IAS 59th Ind. Commercial Power Syst. Tech. Conf.*, 2023, pp. 1–7, doi: 10.1109/ICPS57144.2023.10142087.

[29] B. Taheri, A. Safdarian, M. Moeini-Aghtaie, and M. Lehtonen, "Distribution system resilience enhancement via mobile emergency generators," *IEEE Trans. Power Del.*, vol. 36, no. 4, pp. 2308–2319, Aug. 2021, doi: 10.1109/TPWRD.2020.3007762.

[30] J. M. Home-Ortiz, O. D. Melgar-Dominguez, M. S. Javadi, J. R. S. Mantovani, and J. P. S. Catalão, "Improvement of the distribution systems resilience via operational resources and demand response," *IEEE Trans. Ind. Appl.*, vol. 58, no. 5, pp. 5966–5976, Sep./Oct. 2022, doi: 10.1109/TIA.2022.3190241.

[31] S. Karimi, P. Musilek, and A. M. Knight, "Dynamic Thermal rating of transmission lines: A review," *Renew. Sustain. Energy Rev.*, vol. 91, pp. 600–612, Aug. 2018.

[32] E. Pastor, L. Zarate, E. Planas, and J. Arnaldos, "Mathematical models and calculation systems for the study of wildland fire behavior," *Prog. Energy Combustion Sci.*, vol. 29, pp. 139–153, 2003.
[33] H. T. Nguyen, J. Muhs, and M. Parvania, "Preparatory operation of automated distribution systems for resilience enhancement of critical loads," *IEEE Trans. Power Del.*, vol. 36, no. 4, pp. 2354–2362, Aug. 2021, doi: 10.1109/TPWRD.2020.3030927.
[34] R. A. Jabr, R. Singh, and B. C. Pal, "Minimum Loss network reconfiguration using mixed-integer convex programming," *IEEE Trans. Power Syst.*, vol. 27, no. 2, pp. 1106–1115, May 2012, doi: 10.1109/TPWRS.2011.2180406.
[35] B. Amanulla, S. Chakrabarti, and S. N. Singh, "Reconfiguration of power distribution systems considering reliability and power loss," *IEEE Trans. Power Del.*, vol. 27, no. 2, pp. 918–926, Apr. 2012, doi: 10.1109/TPWRD.2011.2179950.
[36] C.-T. Su and C.-S. Lee, "Network reconfiguration of distribution systems using improved mixed-integer hybrid differential evolution," *IEEE Trans. Power Del.*, vol. 18, no. 3, pp. 1022–1027, Jul. 2003, doi: 10.1109/TPWRD.2003.813641.
[37] "CVX, Matlab software for disciplined convex programming, Version 2.2," Jan. 2020, [Online]. Available: http://cvxr.com/cvx/
[38] S. Mohagheghi and S. Rebennack, "Optimal resilient power grid operation during the course of a progressing wildfire," *Int. J. Elect. Power Energy Syst.*, vol. 73, pp. 843–852, 2015.
[39] L. Economics, "Estimating the value of lost load-briefing paper prepared for the Electric Reliability Council of Texas," 2013.
[40] PVWatts Calculator, 2023. [Online]. Available: https://pvwatts.nrel.gov/index.php
[41] S. Reddy B. and G. Mitra, "Investigations on high temperature low sag (HTLS) conductors," *IEEE Trans. Power Del.*, vol. 35, no. 4, pp. 1716–1724, Aug. 2020, doi: 10.1109/TPWRD.2019.2950992.
[42] Prysmian Group, "TransPowr ACCC/TW bare overhead conductor, trapezoidal aluminum conductor, composite core-concentric-lay-stranded," Jan. 2023. [Online]. Available: https://na.prysmiangroup.com